ISSN 1674-1056
http://cpb.iphy.ac.cn
http://iopscience.iop.org/cpb
中国物理 B
Chinese Physics
中国物理 Chinese Physics B

# *Ab initio* molecular dynamics study on the local structuresin $Ce_{70}Al_{30}$ and $La_{70}Al_{30}$ metallic glasses

F X Li(李福祥), J B Kong(孔吉波), M Z Li(李茂枝)

**Citation:**Chin. Phys. B . 2018, 27(5): 056102. **doi:** 10.1088/1674-1056/27/5/056102

Journal homepage: http://cpb.iphy.ac.cn; http://iopscience.iop.org/cpb

**What follows is a list of articles you may be interested in**

---

## Molecular dynamics simulations of cascade damage near the $Y_2Ti_2O_7$ nanocluster/ferrite interface in nanostructured ferritic alloys

Yi-Qiang Sun(孙祎强), Wen-Sheng Lai(赖文生)
Chin. Phys. B . 2017, 26(7): 076106. **doi:** 10.1088/1674-1056/26/7/076106

## Diffusion and thermite reaction process of film-honeycomb Al/NiO nanothermite: Molecular dynamics simulations using ReaxFF reactive force field

Hua-Dong Zeng(曾华东), Zhi-Yang Zhu(祝志阳), Ji-Dong Zhang(张吉东), Xin-Lu Cheng(程新路)
Chin. Phys. B . 2017, 26(5): 056101. **doi:** 10.1088/1674-1056/26/5/056101

## Relationship between Voronoi entropy and the viscosity of $Zr_{36}Cu_{64}$ alloy melt based on molecular dynamics

Gao Wei, Feng Shi-Dong, Zhang Shi-Liang, Qi Li, Liu Ri-Ping
Chin. Phys. B . 2015, 24(12): 126102. **doi:** 10.1088/1674-1056/24/12/126102

## Molecular dynamics simulation of an argon cluster filled inside carbon nanotubes

Cui Shu-Wen, Zhu Ru-Zeng, Wang Xiao-Song, Yang Hong-Xiu
Chin. Phys. B . 2014, 23(10): 106105. **doi:** 10.1088/1674-1056/23/10/106105

## Mechanical properties of self-irradiated single-crystal copper

Li Wei-Na, Xue Jian-Ming, Wang Jian-Xiang, Duan Hui-Ling
Chin. Phys. B . 2014, 23(3): 036101. **doi:** 10.1088/1674-1056/23/3/036101

---

# *Ab initio* molecular dynamics study on the local structures in $Ce_{70}Al_{30}$ and $La_{70}Al_{30}$ metallic glasses*

F X Li(李福祥), J B Kong(孔吉波), and M Z Li(李茂枝)†

*Department of Physics, Beijing Key Laboratory of Opto-electronic Functional Materials & Micro-nano Devices, Renmin University of China, Beijing* 100872, *China*

(Received 8 February 2018; revised manuscript received 26 February 2018; published online 26 April 2018)

*Ab initio* molecular dynamics simulations were performed to investigate the effect of similar elements on the short- to medium-range atomic packing features in $Ce_{70}Al_{30}$and $La_{70}Al_{30}$glass-forming alloys. 4f electrons of Ce element in $Ce_{70}Al_{30}$ alloy were properly treated in electronic calculations. The local atomic structures in both alloys are qualitatively similar. However, the local environments of Al atoms in $Ce_{70}Al_{30}$ alloy show fluctuation with temperature in the cooling process, which could result from 4f electrons of Ce elements. Surprisingly, the medium-range atomic packing features of Al atoms in both MGs are quite different, although Ce and La elements are similar. These findings are useful for understanding the enhanced glass-forming ability by similar element substitution in RE-based MGs from a medium-range structure perspective.

**Keywords:** rare earth-based metallic glasses, medium-range order, molecular dynamics simulation

**PACS:** 61.20.Ja, 61.25.Mv, 64.70.pe, 64.70.Q– **DOI:** 10.1088/1674-1056/27/5/056102

## 1. Introduction

Recently, rare earth (RE)-based metallic glasses (MGs) have attracted strong interest, because of their valuable scientific problems and technological applications, such as superplasticity, thermoplasticity, high glass-forming ability, and ductility.[1–6] It has been found that Ce-based bulk metallic glasses (BMGs) have exceptionally low glass transition temperature, similar to or lower than that of many polymers, which makes Ce-based BMGs show excellent thermoplastic molding and imprinting ability.[2] This demonstrates that Ce-based BMGs exhibit a superior glass-forming ability (GFA) and high resistance to crystallization over a wide temperature range.[2] In addition, the polymorphic transitions and anomalous compression behavior induced by pressure were also observed in Ce-based BMGs, indicative of the importance of 4f electrons in the Ce element.[7–9] On the other hand, the GFA of La-based alloys can be improved by substituting other lanthanide elements such as Ce.[2] The similar element substitution enhanced GFA in RE-based MGs cannot be understood by conventional criteria such as large atomic size mismatch.[10] This implies that the lanthanide elements with similar atomic sizes and various valence electronic structure may have a significant impact on improving GFA in RE-based glass-forming alloys. *Ab initio* molecular dynamics simulations were performed, which showed that more icosahedral-like clusters and less free volume could be the structural origin of the higher GFA induced by partial substitution of Ce for La in LaCoAl bulk MG.[11] So far, however, the atomic structure features in Ce- and La-based MGs were not fully characterized. How the 4f electrons in the Ce element affect atomic structures has not been addressed yet. It is not clear, either, whether the medium-range atomic packing is also similar in the similar element substitution of Ce and La in RE-based MGs, and whether there is any correlation between medium-range atomic packing and GFA.

In this work, we performed *ab initio* molecular dynamics (MD) simulations to systematically investigate the short- and medium-range structures in $Ce_{70}Al_{30}$ metallic liquids and glasses. Here binary alloy with Ce rich was chosen for simplicity in both simulations and structural analysis. In our simulations, 4f electrons in the Ce element at ambient pressures were modeled by adopting LDA+U calculations. Meanwhile, we also performed *ab initio* MD simulations for $La_{70}Al_{30}$ metallic liquids and glasses in which La has similar valence and ionic radii but without 4f electron. Therefore, the structure features in both $Ce_{70}Al_{30}$ and $La_{70}Al_{30}$ glass-forming alloys can be fully characterized for understanding the effect of similar elements on short- to medium-range atomic structures and thereby GFA.

## 2. Computational details

*Ab initio* MD simulations in the canonical NVT (constant atom number, volume, and temperature) ensemble were performed using the Vienna *ab initio* simulation package (VASP).[12] Projected augmented plane waves (PAW) with the PBE exchange-correlation potential[13] were adopted to describe electron–ion interaction. The simulations were per-

*Project supported by the National Natural Science Foundation of China (Grant Nos. 51631003 and 51271197), the National Basic Program of China (Grant No. 2015CB856800), the Fundamental Research Funds for the Central Universities, China, and the Research Funds of Renmin University of China (Grant No. 16XNLQ01).

†Corresponding author. E-mail: maozhili@ruc.edu.cn

© 2018 Chinese Physical Society and IOP Publishing Ltd 

formed only at the $\Gamma$ point. Cubic supercells containing 200 atoms for $Ce_{70}Al_{30}$ and $La_{70}Al_{30}$ systems were initially constructed with periodic boundary conditions applied in three directions. A stepwise quenching process with a cooling rate of $5 \times 10^{13}$ K/s was adopted to obtain the liquid and glass structures at various temperatures. They were first melted and equilibrated at 1500 K for 2000 MD steps with a time step of 5 fs, and then sequentially equilibrated for 10 ps at each temperature. Before isothermal annealing at each temperature of interest, the supercell volumes were adjusted to give zero pressure. After that, they were further relaxed isothermally for 10000 time steps for the atomic structure analysis. To correctly describe the $f$-electron of the Ce element in $Ce_{70}Al_{30}$ alloy, Dudarev's approach based on the LDA+$U$ theme was adopted with the Hubbard $U$ parameter set to be 5.6 eV,[14] which has been applied to explore polyamorphism in Ce-based MGs.[7]

## 3. Results and discussion

### 3.1. Pair correlation function analysis

Figure 1 shows the temperature evolution of total and partial pair correlation functions (PCFs) in $Ce_{70}Al_{30}$ and

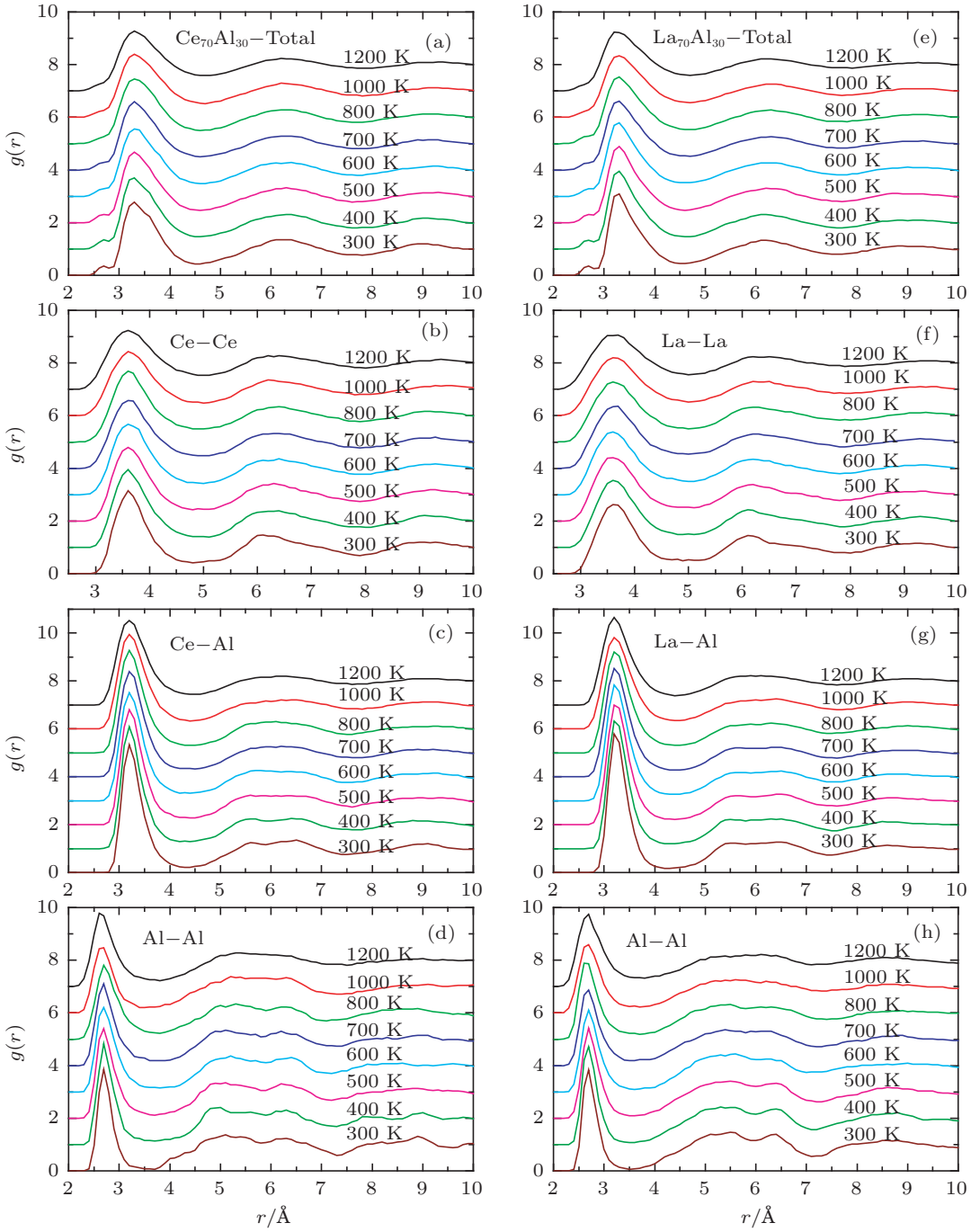



**Fig. 1.** (color online) Total and partial PCFs in (a)–(d) $Ce_{70}Al_{30}$ and (e)–(h) $La_{70}Al_{30}$ glass-forming alloys at various temperatures in the cooling process, respectively.

$La_{70}Al_{30}$ metallic glass-forming alloys in the quenching process, respectively. As temperature decreases, the height of the first peak in total PCFs increases, but the peak position does not change much, as shown in Figs. 1(a) and 1(e). This indicates an increasing degree of short-range order in both glass-forming alloys during cooling. For the second peak, the magnitude also increases slightly. However, it does not show the splitting as observed in CuZr metallic alloy system with decreasing temperature.[15] In addition, a small pre-peak around 2.8 Å in total PCFs is emerging with decreasing temperature, which corresponds to the Al–Al pair and indicates that the short-range order around Al atoms becomes stronger as temperature decreases. As shown in Figs. 1(b) and 1(f), Ce–Ce and La–La partial PCFs are similar to the respective total PCFs. For Ce–Al and La–Al PCFs, however, the first peak becomes much narrower and sharper, as temperature decreases. Moreover, the second peak is getting wider and exhibits splitting at low temperatures. In Al–Al PCFs in both glass-forming alloys, the first peak is located around 2.8 Å, corresponding to the pre-peak in total PCFs shown in Figs. 1(a) and 1(e), respectively. The splitting of the second peak is also observed and becomes more obvious in Al–Al PCFs. Furthermore, more peaks beyond the second peak are developed in both MGs at 300 K. This indicates that significant medium-range order between Al atoms is developed in the cooling process. It can be seen from Figs. 1(d) and 1(h) that Al–Al PCFs in both glass-forming alloys show similar peaks. However, the peak positions are slightly different, which could imply that the medium-range atomic packing of Al atoms in two MGs is different. This will be further characterized and analyzed in Section 3.3.

### 3.2. Voronoi tessellation analysis

To investigate the local atomic structures beyond the PCFs in both $Ce_{70}Al_{30}$ and $La_{70}Al_{30}$ systems, the Voronoi tessellation method was employed, which divides space into close-packed polyhedra around atoms by construction of bisecting planes along the lines joining the central atom and all its neighbors.[16–18] Each Voronoi polyhedron can be identified with the Voronoi index $< n_3, n_4, n_5, n_6 >$ to designate the character of the atomic cluster surrounding an atom, where $n_i$ ($i = 3, 4, 5, 6$) denotes the number of $i$-edged faces in the Voronoi polyhedron. In the Voronoi analysis, atoms sharing faces in their polyhedra are the nearest neighbors, so that the total number of faces in a polyhedron can be used to determine the coordination number (CN) of the central atom. Thus, we first analyzed the average CNs as a function of temperature. Figure 2 shows the distributions of total and partial CNs in both $Ce_{70}Al_{30}$ and $La_{70}Al_{30}$ glass-forming alloys at 1200 K and 300 K, respectively. It can be seen that CN distributions show a slight difference in two systems. As shown in Fig. 2(a), CNs around 13, 14, and 15 are different in two systems. The distributions of CN=13 in two alloys at 1200 K are almost the same. However, the distribution of CN=13 in $La_{70}Al_{30}$ MG at 300 K significantly decreases, but that in $Ce_{70}Al_{30}$ MG at 300 K only decreases a little. The situation is reversed in the distribution of CN=14. It can be seen that the distribution of CN=14 in $Ce_{70}Al_{30}$ alloy decreases more than in $La_{70}Al_{30}$ alloy, as temperature decreases. For the distributions of CN=15, while it decreases in $Ce_{70}Al_{30}$ alloy with decreasing temperature, it increases in $La_{70}Al_{30}$ alloy. From the distributions of partial CNs shown in Figs. 2(b) and 2(c), it can be concluded that the difference in total CN distributions in two alloys is essentially related to the partial CNs around Ce and La atoms in $Ce_{70}Al_{30}$and $La_{70}Al_{30}$ glass-forming alloys, respectively. For the distributions of partial CNs around Al atoms in both alloys, only the distributions of CN=10 and CN=13 at 300 K show the obvious difference. The above results indicate that the local structures in $Ce_{70}Al_{30}$ and $La_{70}Al_{30}$ glass-forming alloys are

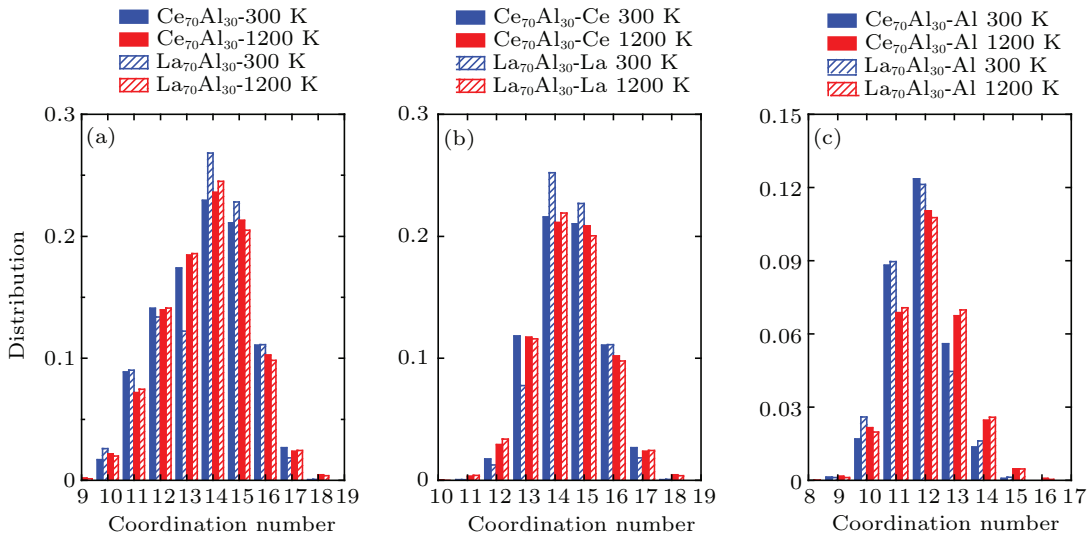



**Fig. 2.** (color online) Total (a) and partial ((b), (c)) coordination numbers in $Ce_{70}Al_{30}$ and $La_{70}Al_{30}$ glass-forming alloys at 1200 K and 300 K, respectively.

a little different, although Ce and La elements are similar and the two glass-forming alloys exhibit almost the same averaged structure features as shown in Fig. 1.

To get more detailed structural information for the local atomic arrangement, we analyzed the bond–angle distribution, the so-called three-body correlation,[18] which characterizes the angles between two bonds connecting the central atom to any two neighboring atoms. Figure 3 shows the total bond-angle distributions for $Ce_{70}Al_{30}$ and $La_{70}Al_{30}$ glass-forming alloys at various temperatures. Both systems exhibit quite similar bond-angle distributions. There are two main peaks located at 55° and 105°. Previous studies have shown that for the icosahedral short-range order, the bond angles are 63.5° and 116.5°,[18] quite different from the two main peak angles shown in Fig. 3. This indicates that the local structure ordering in $Ce_{70}Al_{30}$ and $La_{70}Al_{30}$ glass-forming alloys would not be icosahedral dominated, but quite complex.

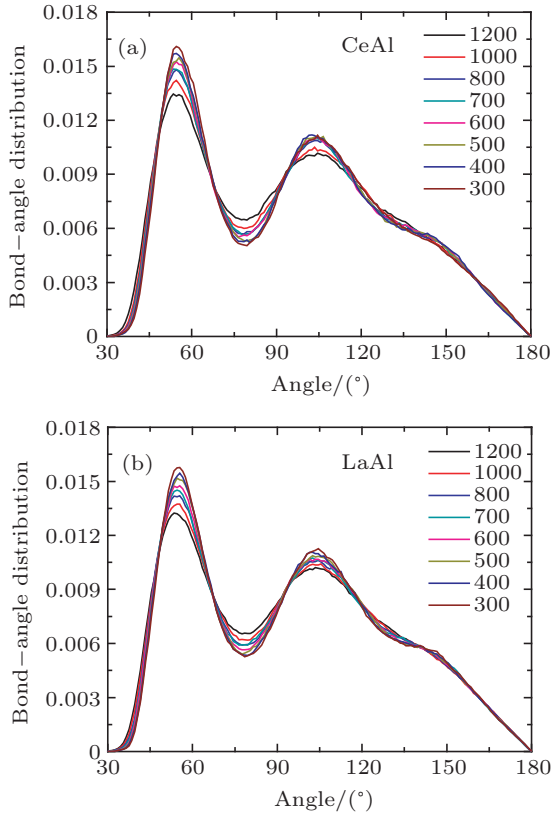



**Fig. 3.** (color online) Total bond-angle distributions in $Ce_{70}Al_{30}$ (a) and $La_{70}Al_{30}$ (b) glass-forming alloys at various temperatures, respectively.

We also investigate the partial bond–angle distributions at various temperatures in $Ce_{70}Al_{30}$ and $La_{70}Al_{30}$ glass-forming alloys, respectively. As shown in Fig. 4(a), the bond angle distribution of Ce–Ce–Ce exhibits a similar behavior to that in the total bond-angle distribution. This indicates that the bond-angle distribution of Ce–Ce–Ce is dominant. On the other hand, another peak located around 150° in Ce–Ce–Ce becomes more obvious as temperature decreases. For Ce–Ce–Al, as temperature decreases, the first peak increases and shifts toward larger angles, from about 51° to 54°. The second and third peaks are located at 100° and 146°, respectively. Although the peak positions in Ce–Ce–Al are different from those in Ce–Ce–Ce, the shape of bond-angle distributions is similar. For Al–Ce–Al, the first and second peaks are located around 48 and 98, shifting towards smaller angles compared to those in Ce–Ce–Al. The third peak located around 150° is getting more pronounced in the distribution of Al–Ce–Al. For La atoms in the $La_{70}Al_{30}$ alloy, the bond angle distributions are similar to those around Ce atoms in the $Ce_{70}Al_{30}$ alloy, as shown in Figs. 4(g), 4(h), and 4(i). In contrast, bond–angle distributions around Al atoms exhibit different behaviors in $Ce_{70}Al_{30}$ and $La_{70}Al_{30}$ glass-forming alloys. For Ce–Al–Ce in the $Ce_{70}Al_{30}$ glass-forming alloy shown in Fig. 4(d), the first peak increases, but the peak position does not change. The two main peaks are located at around 65° and 118°, respectively, which are quite close to the icosahedral bond angles[18]. This indicates that the Ce atoms around Al atoms are arranged in an icosahedral-like fashion. The bond angles of La–Al–La in $La_{70}Al_{30}$ alloy show similar distributions. For Al–Al–Ce, the first peak splits into two peaks with decreasing temperature, located at around 49° and 63°, respectively. However, the intensities of these two peaks do not change monotonically with temperature, but show fluctuation with temperature. Finally, in $Ce_{70}Al_{30}$ MG at 300 K, two peaks are formed. This implies that the arrangement of Al and Ce atoms around Al atoms is affected significantly by temperature in glass formation. This is totally different in bond-angle distributions of Al–Al–La in $La_{70}Al_{30}$ alloy. As shown in Fig. 4(k), the distribution at 1200 K exhibits the main peak around 60° with a shoulder on the left. As temperature decreases, the main peak becomes narrower and shifts to around 63°, and the intensity increases continuously with decreasing temperature. Meanwhile, a small peak on the left is gradually formed, and the intensity increases with temperature decrease. This indicates that the arrangements of Al and La atoms around Al atoms in the$La_{70}Al_{30}$ alloy are relatively stable, so that the bond-angle distribution of Al–Al–La changes continuously in the cooling process. Such features are also reflected in the bond-angle distributions of Al–Al–Al. As shown in Fig. 4(f), the distribution of Al–Al–Al in the $Ce_{70}Al_{30}$ alloy does not change monotonically with temperature, either. At some temperatures, there is only a main peak around 60° with a shoulder on the left. At some other temperatures, there are two small peaks located around 42° and 60°, respectively. In $La_{70}Al_{30}$ alloy, however, two small peaks around 42° and 60° are formed gradually with decreasing temperature, as shown in Fig. 4(l). In addition, a peak located around 170° becomes more obvious, which is not observed in the $Ce_{70}Al_{30}$ alloy. Although Ce and La atoms are similar, the local atomic configurations of Al atoms in these two systems show a significant difference.

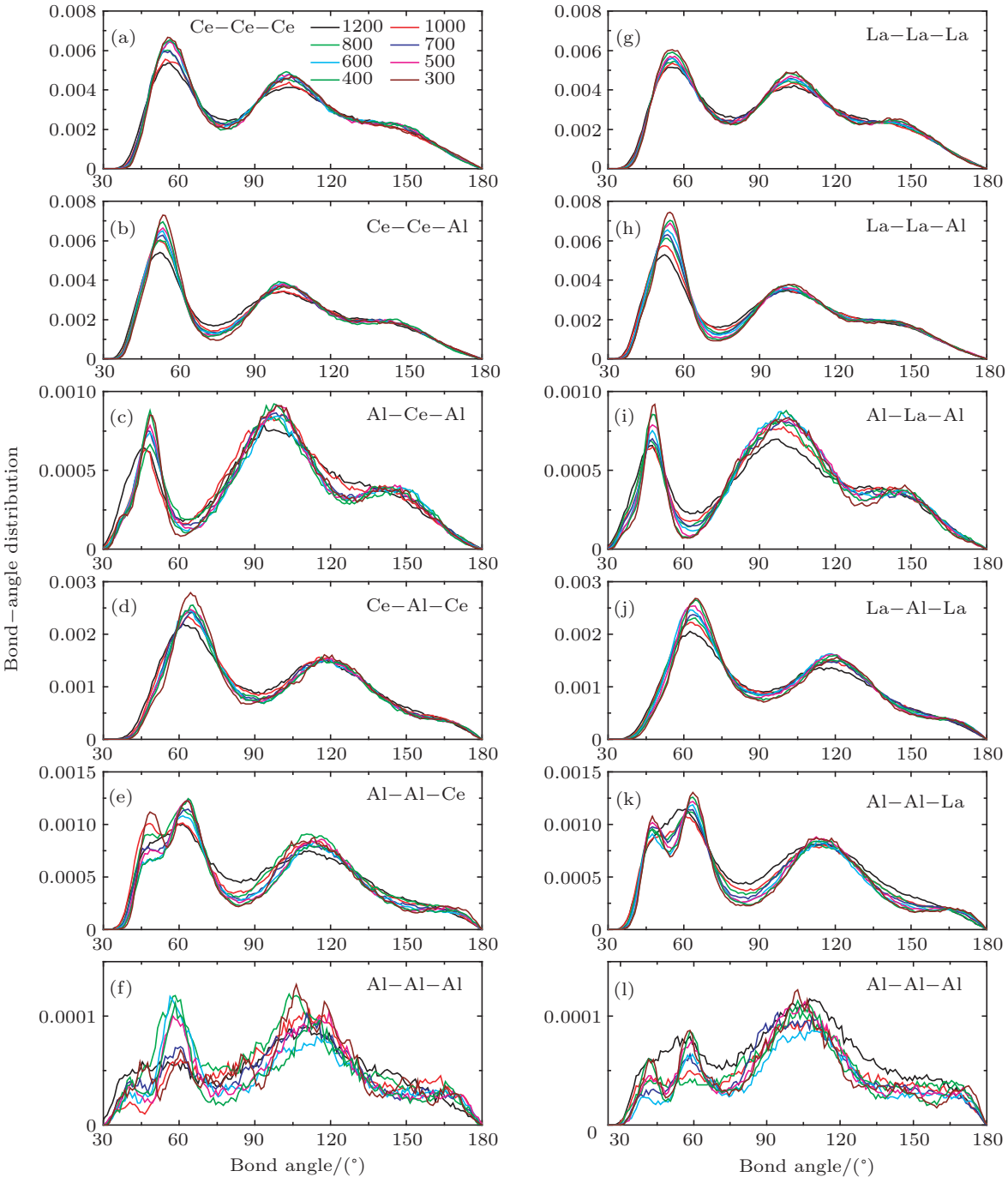



**Fig. 4.** (color online) Partial bond–angle distributions in $Ce_{70}Al_{30}$ ((a)–(f)) and $La_{70}Al_{30}$ ((g)–(l)) glass-forming alloys at various temperatures, respectively.

According to the above analysis, the local atomic arrangements related to Al atoms change significantly as temperature decreases. In addition, the local structures around Al atoms are also different in $Ce_{70}Al_{30}$ and $La_{70}Al_{30}$ glass-forming alloys. To get a deeper insight into the local atomic structure features, we analyzed the distributions of the major populated atomic clusters in $Ce_{70}Al_{30}$ and $La_{70}Al_{30}$ glass-forming alloys at various temperatures. It is found that Ce (La) and Al atoms in $Ce_{70}Al_{30}$($La_{70}Al_{30}$) alloy rarely share the same types of atomic clusters, so that only the major populated Ce (La)-centered and Al-centered atomic clusters were presented, respectively, as shown in Fig. 5. It can be seen that the major atomic clusters are slightly different for Ce and La atoms, as shown in Figs. 5(a) and 5(c), respectively. For Ce atoms, $\langle 0,0,12,0\rangle$ is the only type of 12-coordinated cluster. For La atoms, however, $\langle 1,3,5,3\rangle$ as well as $\langle 0,0,12,0\rangle$ are 12-coordinated clusters. The population of both Ce-centered and La-centered $\langle 0,0,12,0\rangle$ clusters is very small. However, the fraction of La-centered $\langle 1,3,5,3\rangle$ clusters is much larger. On the other hand, Ce-centered clusters also contain 13-coordinated $\langle 1,3,4,5\rangle$ and 16-coordinated $\langle 0,2,8,6\rangle$ clusters, but no such clusters are major populated around La atoms.

In addition, La atoms in $La_{70}Al_{30}$ alloy contain one more type of 14-coordinated clusters, $\langle 0,4,5,5\rangle$. For Al-centered clusters, only the 13-coordinated clusters are different in these two systems. In $Ce_{70}Al_{30}$ alloy, the 13-coordinated cluster is $\langle 1,2,5,5\rangle$, while in $La_{70}Al_{30}$ alloy the 13-coordinated cluster is $\langle 0,3,6,4\rangle$. The fraction of $\langle 0,3,6,4\rangle$ is much more than that of $\langle 1,2,5,5\rangle$. Therefore, in the $La_{70}Al_{30}$ alloy, Al atoms tend to form $\langle 0,3,6,4\rangle$ and $\langle 0,2,8,2\rangle$, which are often regarded as icosahedral-like clusters.[18] For other types of clusters, they are all major populated in both alloys. Although their fractions show a little difference, the temperature dependent behaviors are similar. In both alloys, most $\langle 0,0,12,0\rangle$ clusters are Al-centered. However, the fraction of icosahedral clusters is very small in these two systems, indicating that icosahedral clusters are not dominated local structures, consistent with the above analysis. This is in contrast to CuZr metallic glass-forming alloy where the population of $\langle 0,0,12,0\rangle$ is dominant. The Voronoi analysis further demonstrates that the local atomic structures show a little difference, although Ce and La atoms are quite similar.

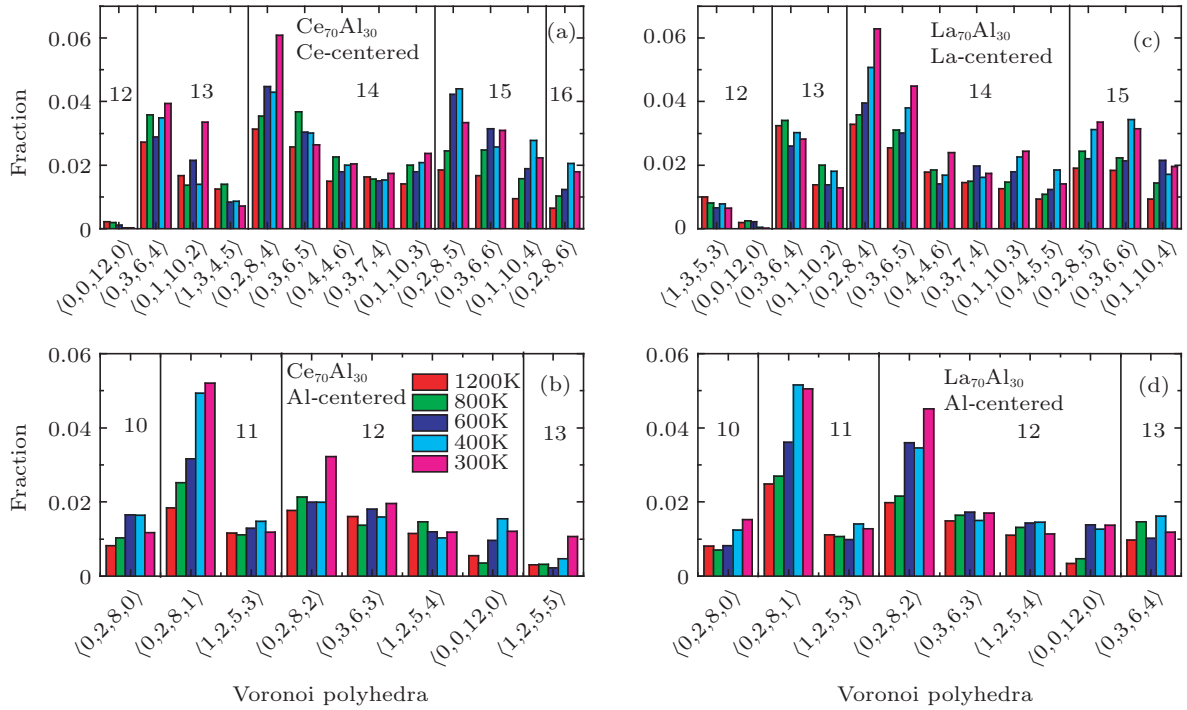



**Fig. 5.** (color online) Fraction of the major populated atomic clusters in $Ce_{70}Al_{30}$ ((a), (b)) and $La_{70}Al_{30}$ ((c), (d)) glass-forming alloys at various temperatures, respectively.

### 3.3. Medium-range atomic packing analysis

As mentioned above, in partial PCFs of the Al–Al pair in $Ce_{70}Al_{30}$ and $La_{70}Al_{30}$ alloys, the peak positions show a slight difference, indicative of different atomic packing in medium-range structures in two MGs. To further characterize the medium-range atomic packing features in two MGs, we analyzed the partial PCFs with the distance scaled by the first peak position $R_1$. Previous studies show that the oscillation in the PCFs is an indication that a certain order does exist in amorphous solids, and the values of $R_i/R_1$ ($i = 1$, 2, 3, 4, 5) in PCFs correspond to several characteristic constants of $\sqrt{1}$, $\sqrt{3}$, $\sqrt{4}$, $\sqrt{7}$, and $\sqrt{12}$.[19] Further studies reveal that the scaled peak positions of partial PCFs in MGs reflect medium-range atomic packing orders.[20,21] For multicomponent MGs, the scaled peak positions of partial PCFs may correspond to different sequences of characteristic constants, indicative of different medium-range topological orders, which are found to directly correlate with the glass-forming ability.[18] Therefore, we analyzed the scaled partial PCFs in $Ce_{70}Al_{30}$ and $La_{70}Al_{30}$ MGs to investigate the medium-range atomic packing feature.

Figure 7 shows the scaled partial PCFs for Ce–Ce, Ce–Al, and Al–Al in $Ce_{70}Al_{30}$ MG and La–La, La–Al, and Al–Al in $La_{70}Al_{30}$ MG, respectively. It can be seen that the scaled PCFs of Ce–Ce and La–La are quite similar. The peak positions are almost the same. However, the scaled PCFs of Ce–Al and La–Al, Al–Al ($Ce_{70}Al_{30}$) and Al–Al ($La_{70}Al_{30}$) are significantly different. For Ce–Al and La–Al pairs, the second and third peak positions are almost the same. However, the fourth peak positions are quite different, located at $\sqrt{8}$ and $\sqrt{7}$ in Ce–Al and La–Al pairs, respectively. For La–Al pair, the fifth peak is not obvious, while it still exhibits significant ordering in Ce–Al pair. This indicates that the medium-range atomic packing for Ce–Al and La–Al is different, and medium-range order between Ce and Al in $Ce_{70}Al_{30}$ MG is more significant than that between La and Al in $La_{70}Al_{30}$ MG. Furthermore, the scaled Al–Al partial PCFs in both MGs are also quite different in both peak positions and peak number. It can be seen that at $R/R_1 \approx \sqrt{3}$, there is a small shoulder in Al–Al of $Ce_{70}Al_{30}$ MG, but no peak or shoulder shows up in Al–Al of $La_{70}Al_{30}$

MG. On the contrary, at $R/R_1 \approx \sqrt{8}$, there is a small shoulder in Al–Al of $La_{70}Al_{30}$ MG. As $R/R_1$ is close to $\sqrt{4}$ and $\sqrt{16/3}$, the scaled Al–Al partial PCFs in both MGs show two peaks, respectively. However, the peak intensities in $La_{70}Al_{30}$ MG are higher. There are even two more peaks at $R/R_1 \approx \sqrt{11}$ and $\sqrt{40/3}$ in Al–Al of $Ce_{70}Al_{30}$ MG. However, there is only one peak located at $R/R_1 \approx \sqrt{10}$ in Al–Al of $La_{70}Al_{30}$ MG, which is also different from the peak of $R/R_1 \approx \sqrt{11}$ in Al–Al of $Ce_{70}Al_{30}$ MG. Therefore, the medium-range atomic packing related to Al atoms in two MGs is significantly different, although Ce and La are similar elements and the compositions in two MGs are the same. This is different from the MGs with a large atomic size mismatch.

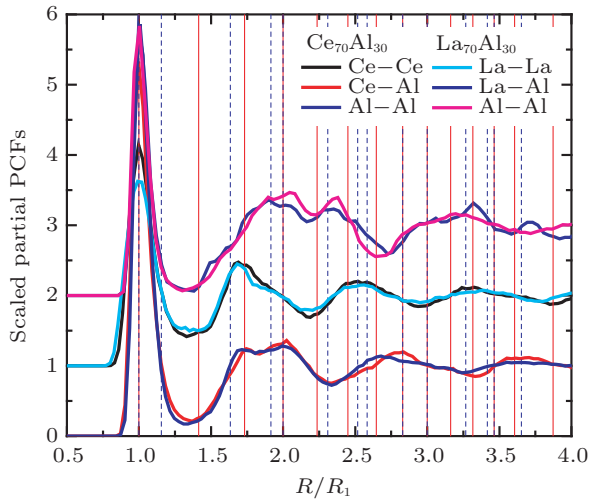



**Fig. 6.** (color online) Scaled partial pair correlation functions in $Ce_{70}Al_{30}$ and $La_{70}Al_{30}$ MGs at 300 K, respectively.

Recently, similar element substitution enhanced GFA was observed by substitution of Ce for La in $(La_{0.7}Ce_{0.3})_{65}Co_{25}Al_{10}$ bulk MGs.[3] It was found that more icosahedral-like clusters may be one of the structural origins of the higher GFA enhanced by similar element substitution.[9] This is consistent with the above local structure analysis in terms of the Voronoi tessellation method. The substitution of Ce for La will introduce more $\langle 0,3,6,4\rangle$ and $\langle 0,1,10,2\rangle$ icosahedral-like atomic clusters, since such clusters tend to form around Ce atoms, which may play different roles in dynamical properties as liquids are quenched into glassy states.[22] More importantly, the medium-range atomic packing analysis shows that the substitution of Ce will introduce more different atomic packing in medium range structures. Although Ce and La atoms are similar, their medium-range atomic packing with Al is quite different, as shown in Fig. 6. In addition, the substitution of Ce atoms will also lead to the more complicated atomic packing of Al atoms in medium-range structures. More diverse medium-range atomic packing introduced by the substitution of Ce for La will enhance GFA in this system. Although Ce and La are similar, the Ce element contains 4f electrons, which could be the physical reason for the distinctive short- to medium-range atomic packing in $Ce_{70}Al_{30}$ and $La_{70}Al_{30}$MGs and enhanced GFA by similar element substitution. This also implies that a slight difference may lead to a significant difference in short- to medium-range atomic packing.

## 4. Conclusion

In summary, we performed systematic *ab initio* MD simulations for $Ce_{70}Al_{30}$ and $La_{70}Al_{30}$ glass-forming alloys. The short-range local atomic structures exhibit a little difference, especially for the local structures of Al atoms, which could result from the 4f electrons in the Ce element. More importantly, the medium-range atomic packing between Al atoms in both MGs is significantly different, although Ce and La are similar elements, which may be the key underlying structural basis for the enhanced GFA by similar element substitution in RE-based MGs.

## References

[1] Guo F and Poon S J 2003 *Appl. Phys. Lett.* **83** 2575
[2] Zhang B, Zhao D Q, Pan M X, Wang W H and Greer A L 2005 *Phys. Rev. Lett.* **94** 205502
[3] Li R, Pang S J, Men H, Ma L C and Zhang T 2006 *Scripta Mater.* **54** 1123
[4] Tan H, Zhang Y, Ma D, Feng Y P and Li Y 2003 *Acta Mater.* **51** 4551
[5] Zhang T, Tsai A P, Inoue A and Masumoto T 1992 *Sci. Rep. RITU A* **36** 261
[6] Yu P, Wang R J, Zhao D Q and Bai H Y 2007 *Appl. Phys. Lett.* **91** 201911
[7] Sheng H W, Liu H Z, Cheng Y Q, Wen J, Lee P L, Luo W K, Shastri S D and Ma E 2007 *Nat Mater.* **6** 192
[8] Zeng Q S, Ding Y, Mao W L, Yang W, Sinogeikin S V, Shu J F, Mao H K and Jiang J Z 2010 *Phys. Rev. Lett.* **104** 105702
[9] Zeng Q S, Li Y C, Feng C M, Liermann P, Somayazulu M, Shen G Y, Mao H K, Yang R, Liu J, Hu T D and Jiang J Z 2007 *PNAS* **104** 13565
[10] Wang W H 2007 *Prog. Mater. Sci.* **52** 540
[11] Li X and Zhang T 2017 *J. Appl. Phys.* **122** 085103
[12] Kresse G and Furthmüller J 1996 *Mater. Sci.* **6** 15
[13] Perdew J P, Burke K and Ernzerhof M 1996 *Phys. Rev. Lett.* **77** 3865
[14] Dudarev S L, Botton G A, Savrasov S Y, Humphreys C J and Sutton A P 1998 *Phys. Rev. B* **57** 1505
[15] Hu Y C, Li F X, Li M Z, Bai H Y and Wang W H 2015 *Nat Commun.* **6** 8310
[16] Finney J L 1970 *Proc. R. Soc. London Ser. A* **319** 479
[17] Li M Z, Wang C Z, Hao S G, Kramer M J and Ho K M 2009 *Phys. Rev. B* **80** 184201
[18] Cheng Y Q and Ma E2011 *Prog. Mater. Sci.* **56** 379
[19] Liu X J, Xu Y, Hui X, Lu Z P, Li F, Cheng G L, Lu J and Liu C T 2010 *Phys. Rev. Lett.* **105** 155501
[20] Wu Z W, Li M Z, Wang W H and Liu K X 2015 *Nat Commun.* **6** 6035
[21] Wu Z W, Li M Z, Xu L M and Wang W H 2017 *Acta Phys. Sin.* **66** 176405 (in Chinese)
[22] Li F X and Li M Z 2017 *J. Appl. Phys.* **122** 225103